Ultrafast saturation of resonant optical processes

Anil K. Patnaik,[1,2,*] Sukesh Roy,[3] and James R. Gord[1]
[1]*Air Force Research Laboratory, Aerospace Systems Directorate, Wright-Patterson AFB, Ohio 45433, USA*
[2]*Department of Physics, Wright State University, Dayton, Ohio 45435, USA*
[3]*Spectral Energies, LLC, 5100 Springfield Street, Suite 301, Dayton, Ohio 45431, USA*
(Received 12 June 2014; revised manuscript received 24 October 2014; published 10 December 2014)

A generalized formulation is presented for determining the saturation thresholds for optical processes excited by ultrafast pulses based on the pulse area of the excitation pulse. It is demonstrated that the threshold of driving-pulse intensity for absorption and fluorescence saturation in a two-level system is inversely proportional to the square of the duration of the excitation pulse. These results are obtained from both a simplified analytical solution assuming a Gaussian excitation pulse shape and a detailed numerical calculation based on density-matrix equations. The calculation is generalized further to obtain the saturation condition for a two-photon Raman process by defining a two-photon pulse area both analytically and numerically. These results not only provide predictive capabilities for determining thresholds of signal saturation using ultrashort durations with arbitrary pulse shapes and durations but also open up possibilities for predetermining the threshold intensities of various resonant nonlinear processes.

DOI: 10.1103/PhysRevA.90.063813 PACS number(s): 42.65.Dr, 42.65.Re, 42.50.Gy, 82.53.Kp

I. INTRODUCTION

An atomic or molecular transition saturates when it is pumped to reach an underdamped regime, modifying the absorption spectrum with a saturation dip and Stark shift (Lamb dip) in a homogeneously (inhomogeneously) broadened medium [1]. Typically, a strong cw pump (long-pulse pump laser with a duration longer than the characteristic decays of the system) equalizes the population of a homogeneously broadened two-level system (TLS) in a few Rabi cycles to reach a steady-state (quasisteady state) saturation of absorption with absorption coefficient $\alpha = \alpha_0(1 + I_0/I_s)^{-1}$ [2]. Here, α_0 is the linear absorption coefficient, and I_0 and I_s are the peak laser and saturation intensities, respectively. In the time domain, molecular population and coherence oscillate at a rate known as the Rabi frequency Ω, which is proportional to the square root of the driving-field intensity. When the Rabi frequency Ω exceeds the rates of population decay γ and pure dephasing of coherence Γ associated with the transitions of interest, the system reaches an underdamped regime, i.e.,

$$\Omega > \sqrt{\gamma\Gamma}, \tag{1}$$

and the transition saturates [3]. This condition is pictorially depicted in Fig. 1(a).

However, if the duration of the excitation pulse is shorter than the molecular decay and dephasing time scales and the threshold Rabi period Ω_{cw}^{-1} [as shown in Fig. 1(b)], even in the underdamped regime, this pulse escapes the interaction region long before a steady-state (or a quasisteady-state) absorption saturation is reached. Thus, the question to be addressed is, can absorption be saturated at all in the ultrafast regime? If yes, how? Clearly, inequality (1) is a necessary condition for ultrafast absorption saturation but *no longer a sufficient condition*. In fact, we found that a stronger drive pulse with increased Rabi oscillations within the duration of the drive pulse [as depicted in Fig. 1(c)] can force the system to saturate. For excitations with durations shorter than the decay and dephasing time scales of the system, McCall and Hahn showed that self-induced transparency is achieved along the propagation direction z when the area under the pump pulse, known as *pulse area*,

$$\theta(z) = \int_{-\infty}^{\infty} \Omega(z,t)dt, \tag{2}$$

is larger than π [4]. Here, $\Omega(z,t)$ is the Rabi frequency associated with the pump pulse. Thus, the pulse-area description can clearly be used to obtain a saturation criterion for ultrafast absorption processes. Many interesting pulse-area-based propagation studies have been documented in the literature [5,6]. For shorter pulses, the pulse-area theorem has been revisited [7,8]. The area theorem has also been used to describe the temporal dynamics of accurate control of the quantum states, e.g., in realizing fast quantum gates [9].

From the spectroscopy perspective, ultrashort pulses associated with very high peak powers have been extremely useful for varieties of time-resolved, nonlinear spectroscopic techniques [10]. Generally, these approaches can be classified as below-saturation-threshold [11] and above-saturation-threshold [12] time-resolved spectroscopies. In either case it is crucial to have prior knowledge of the parameter domain leading to the saturation limit before designing an experiment. It has been shown recently that saturation of the molecular N_2 Raman transition with a 100-fs pulse requires a pump intensity that is more than six orders of magnitude stronger than that for a nanosecond-duration pulse [13].

In this paper, our goal is to establish a criterion and determine a scaling law characterizing the saturation threshold for the ultrafast regime, such as Eq. (1) for the long-pulse regime. We use the pulse-area interpretation to obtain the scaling law for single-photon processes such as absorption and emission [Fig. 2(a)]. We also define a two-photon pulse area to obtain a criterion for saturation in Raman scattering [Fig. 2(b)]. We demonstrate that unlike in the cw or long-pulse regimes, an *ultrafast, nonequilibrium, and dynamical*

*anil.patnaik@wright.edu

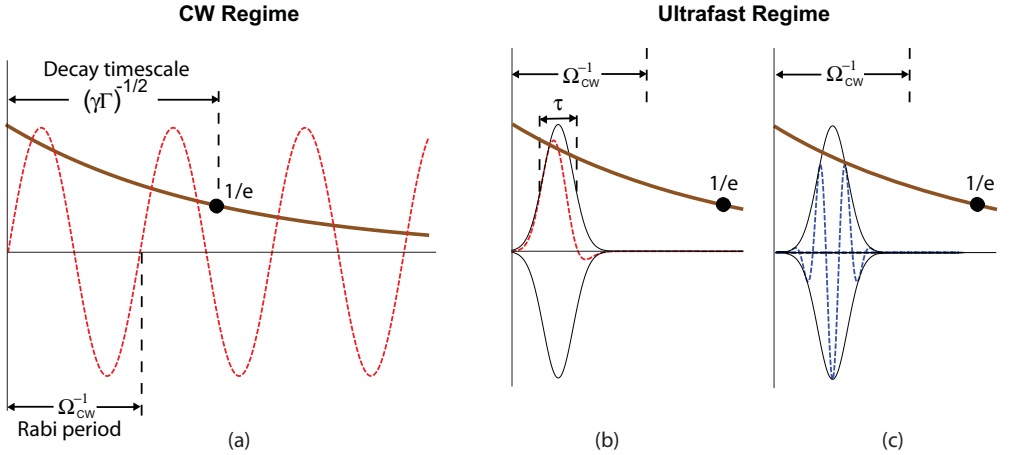

FIG. 1. (Color online) (a) Typical Rabi period Ω_{cw}^{-1} associated with the threshold drive intensity for steady-state absorption saturation in the cw regime is smaller than the effective decay time scale $(\gamma\Gamma)^{-1/2}$. (b) In pulsed excitation, when the duration of excitation is shorter than Ω_{cw}^{-1} (i.e., $\tau < \Omega_{cw}^{-1}$), then even if the peak Rabi frequency of the drive pulse matches Ω_{cw}, the pulse leaves the interaction region way before completion of a single Rabi cycle. Thus, saturation cannot occur. (c) A stronger drive intensity with higher peak intensity can drive multiple Rabi cycles within the pulse to obtain a dynamical saturation of absorption.

saturation can be realized only in the highly underdamped regime. The physics of such a saturation process is very rich because the Rabi-oscillation time scale becomes comparable to that of the vibrational time scale of the molecules. Also, the predictive capability achieved from this result will be extremely useful for establishing design parameters both for saturation-spectroscopy experiments and for experiments that must be operated below saturation limits. This calculation may also be useful for saturation-based ultrafast optical switching and controllable wave-packet dynamics [14].

In Sec. II, we describe a generalized scheme for obtaining the saturation criterion for ultrafast excitations. As an example of the criterion, in Sec. III, we demonstrate its validity in the saturation of absorption and fluorescence in a TLS. In Sec. IV, we define the two-photon pulse area and determine a scaling law for saturation of Raman transition. We summarize the results and outlook in Sec. V.

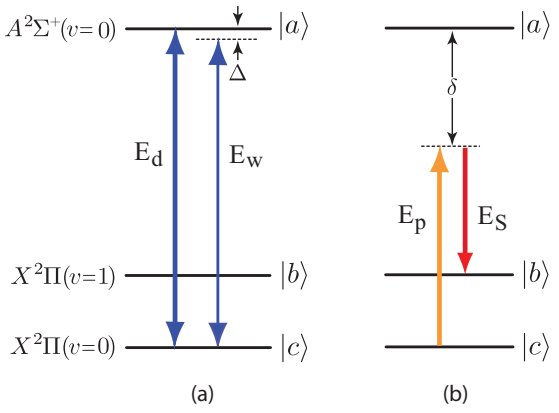

FIG. 2. (Color online) Three-level model scheme depicting energy levels of NO used for studying saturation. (a) Only two levels are used for studying the saturation of absorption of the weak probe pulse $E_w(t)$ and fluorescence by the strong drive pulse $E_d(t)$. (b) The level diagram for investigating the saturation of Raman coherence by the pump pulse E_p and Stokes pulse E_S that are detuned by δ from the excited electronic state.

II. SATURATION IN THE ULTRAFAST EXCITATION REGIME

Let us consider that a system pumped by a resonant ultrashort Gaussian pulse with peak electric field E_{i0} at $t = t_{i0}$, central frequency at ν_i, and pulse duration τ_i can be written as $E_i(t) = E_{i0}e^{-(t-t_{i0})/\tau_i^2}e^{-i\nu_i t} + \text{c.c.}$ The coupling strength of the field with the system is given by Rabi frequency $2\Omega_i = 2\wp_{\alpha\beta}|E_i(t)|/\hbar$, where $\wp_{\alpha\beta} = \langle\alpha|\wp|\beta\rangle$ is the dipole-matrix element between states $|\alpha\rangle$ and $|\beta\rangle$ and $\hbar$ is the Planck constant. Since the amplitude of an ultrafast pulse rapidly evolves in time, a transient pulse area

$$\theta_i(t) = \int_{-\infty}^{t} 2\Omega_i(t')dt' \tag{3}$$

can be defined to characterize the evolving interaction of the pulse and the medium. For a Gaussian pulse, the area of one complete pulse is given by

$$\Theta_i = \lim_{t\to\infty}\theta_i(t) = 2\Omega_{i0}\tau_i\sqrt{\pi}, \tag{4}$$

where, according to McCall and Hahn [4], a transparency is induced in the medium for $\Theta_i \geqslant \pi$. Thus, the above equation can be used to determine the saturation-threshold condition in a variety of processes involving ultrafast interactions. Note the same procedure can be extended to other pulse shapes. Nonadiabatic coupling of TLS with ultrashort pulses of different pulse shapes has shown different behaviors in terms of their transition probabilities [15].

In the following sections, we consider elementary optical processes, such as absorption, emission, and Raman scattering, and determine their saturation criterion analytically based on calculation of the pulse area. We show that for any pulsed resonant excitation with an arbitrary ultrafast duration shorter than the decay and dephasing time scales of the material medium, a generalized criterion for the saturation threshold can be derived. Note that the Rabi period considered in this work is larger than the optical period, and thus, the rotating-wave approximation (RWA) is valid [16]. Also, this

study assumes the interaction volume consists of a thin optical medium or a single molecule.

III. SATURATION THRESHOLDS OF ABSORPTION AND FLUORESCENCE IN A TWO-LEVEL SYSTEM

Let us consider the saturation of absorption and fluorescence in the two-level subsystem shown in Fig. 2(a). The energy levels under consideration are representative of electronic states $X\,^2\Pi$ and $A\,^2\Sigma^+$ of a nitric oxide molecule. The system is driven by the pulse $E_d(t)$, with a central frequency resonant to the $|a\rangle \leftrightarrow |c\rangle$ transition, and is probed by a weak pulse $E_w(t)$ with a detuning Δ from the transition. The pulse-duration dependence is studied parametrically by varying τ_i $(i \to d, w)$ corresponding to the electric-field envelopes. We assume the decay rates of the excited and ground states are same, i.e., $\gamma_{aa} = \gamma_{cc} = \gamma$. The dephasing rate $\gamma_{ac} = \gamma + \Gamma$ determines the coherence decay. For NO the collisional population-decay rates of both states are $\gamma \sim 10^{10}$ s^{-1}, and the pure dephasing rates are $\Gamma \sim 15 \times 10^{10}$ s^{-1} [17]. The spontaneous decay is very slow ($\sim 10^6$ s^{-1}) compared to other decay processes and hence is ignored. Also, collisional quenching is neglected here.

The transient Rabi frequency changes rapidly over the duration of the pulse. During the transient evolution of the drive pulse acting on the TLS, the integrated-absorption and integrated-fluorescence signals

$$A_{\rm int}(t) \propto \int_{-\infty}^{t} {\rm Im}\eta_{ac}(t')dt', \qquad F_{\rm int}(t) \propto \int_{-\infty}^{t} \rho_{aa}(t')dt', \tag{5}$$

respectively, are calculated numerically. Here, ρ_{ij} is the density-matrix element corresponding to the population (coherence) for $i = j$ $(i \neq j)$. Note that since both the drive and the weak probe pulses act on the same transition, we have made the following transformation of the off-diagonal element of the density matrix for extracting the drive-induced molecular polarization experienced by the probe pulse [17]:

$$\rho_{ac}(t) \to \sigma_{ac}(t)e^{-i\nu_d t} + \eta_{ac}(t)e^{-i\nu_w t}. \tag{6}$$

Here, Imη_{ac} determines the absorption of the probe by the TLS, and σ_{ij} corresponds to the polarization experienced by the drive field. After we substitute this transformation, the density-matrix equations for the model system become

$$\begin{aligned}
\dot{\rho}_{aa} &= -\gamma_{aa}\rho_{aa} + [-i\Omega_d^*\sigma_{ac} - i\Omega_w^*\eta_{ac} + {\rm c.c.}],\\
\dot{\sigma}_{ac} &= -\gamma_{ac}\sigma_{ac} + i\Omega_d(\rho_{cc} - \rho_{aa}),\\
\dot{\eta}_{ac} &= -(\gamma_{ac} + i\Delta)\eta_{ac} + i\Omega_w(\rho_{cc} - \rho_{aa}),\\
\dot{\rho}_{cc} &= \gamma_{aa}\rho_{aa} - \gamma_{cc}\rho_{cc} + [i\Omega_d^*\sigma_{ac} + i\Omega_w^*\eta_{ac} + {\rm c.c.}].
\end{aligned} \tag{7}$$

In the absence of the probe field, for a nondecaying system, the solutions for the excited-state population and coherences, respectively, are well known as [18]

$$\rho_{aa}(t) = \sin^2[\theta_d(t)/2], \qquad \sigma_{ac}(t) = \frac{i}{2}\sin[\theta_d(t)]. \tag{8}$$

Here, $\theta_d(t)$ is the transient pulse area defined in Eq. (3), with $i \to d$. Thus, Rabi oscillations occur in the TLS; however, the oscillation frequency is determined by θ_d rather than the Rabi frequency Ω_d itself, unlike in the long-pulse- or the cw-laser excitation regime. For completeness, we plot the full numerical solution of ρ_{aa} and η_{ac} without any approximation in Fig. 3. The temporal evolution of the population ρ_{aa} and coherence η_{ac} matrix elements is calculated by solving the coupled density-matrix equations using the fourth-order Runge-Kutta method. The parameters used for the numerical plots are pulse durations $\tau_d = \tau_w = 100$ fs, centered at $t_{d0} = t_{w0} = 400$ fs, and the peak intensity of the pump (probe) $I_{d0} = 10^{17}$ W/m^2 ($I_{w0} = 10^{10}$ W/m^2). Clearly, in Fig. 3(a), the frequency of oscillation changes as a function of time for both population and coherence. However, when ρ_{aa} and η_{ac} are plotted as a function of the transient pulse area $\theta_d(t)$, the oscillation frequency remains constant and also follows the approximate solution given in Eqs. (8). Note that since the probe is weak, the probe coherence $\eta_{ac}(t)$ follows the coherence $\sigma_{ac}(t)$ generated by the strong drive pulse. It is shown that the efficiency of population transfer and the adiabatic following are modified strongly if propagation of the pulse in a resonant TLS is considered [19]. Rabi oscillations via ultrafast laser excitation of TLS are reported for free-induction decay [20] and fluorescence [21,22].

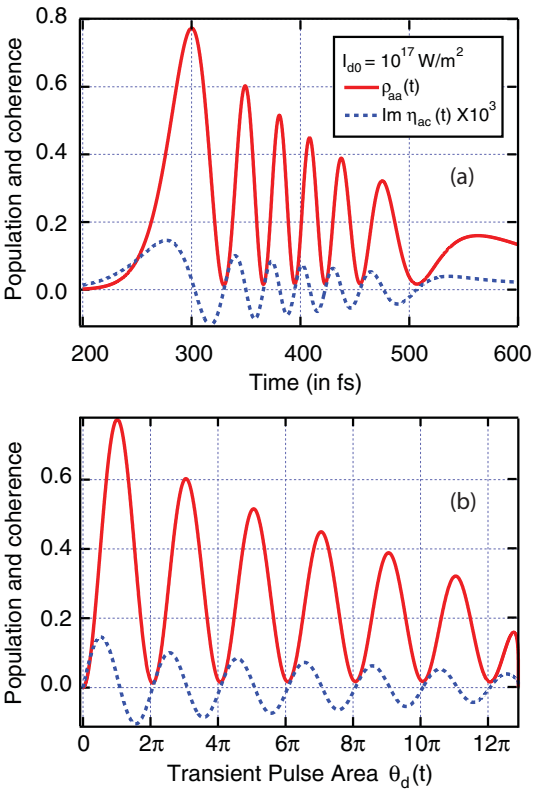

FIG. 3. (Color online) (a) Excited-state population ρ_{aa} and coherence in probe polarization η_{ac} in two-level system as a function of (a) time and (b) transient pulse area $\theta_d(t)$ associated with the drive pulse. Here, $\tau_d = \tau_w = 100$ fs, the peak of the pulses appear at 400 fs, $I_{d0} = 10^{17}$ W/m^2, and $I_{w0} = 10^{10}$ W/m^2.

From the spectroscopy perspective, the Rabi oscillations modify the spectroscopic signature of the transition, creating new peaks in the spectrum. For example, in cw-laser-based

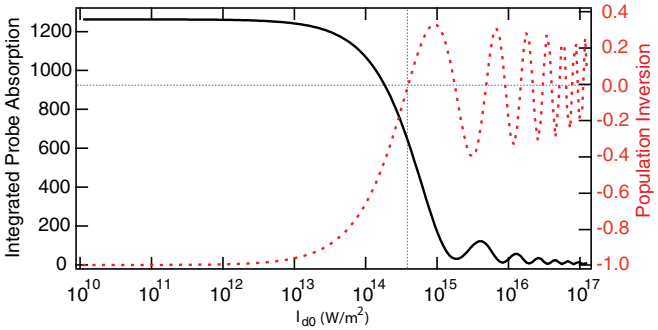

FIG. 4. (Color online) Integrated probe absorption (solid black line) and population (dotted red line) plotted as a function of the peak intensity of the drive field for pulses with pulse duration $\tau_d = 100$ fs.

saturation, two new absorption peaks emerge symmetrically on both sides of the central absorption frequency in the molecular spectrum with reduced absorption at the transition frequency [23]. While such a saturation dip in the absorption spectrum is essential for experiments that exploit the reduced absorption or the associated anomalous dispersion at the central frequency [24], the modified spectrum is detrimental to experiments that rely on the molecular spectroscopic fingerprints for sensing applications [25]. For an ultrafast excitation, the electric field E_d rapidly varies within the duration of the pulse, and so does the probe absorption. Hence, we calculate the integrated probe absorption $A_{\rm int}$ and plot it in Fig. 4 to investigate where and how the ultrafast saturation of absorption occurs. $A_{\rm int}$ (solid black line) is plotted as a function of I_{d0} with pulse durations $\tau_d = \tau_w = 100$ fs. It is clear that for an initial increase of I_{d0} by several orders of magnitude up to 10^{14} W/m^2, $A_{\rm int}$ is reduced by only 10%, but within the next order of magnitude increase from 10^{14} to 10^{15} W/m^2, $A_{\rm int}$ is reduced by two orders of magnitude. To explain this observed dip using molecular population, in the same graph we plot the value of the population inversion $[\rho_{aa}(t) - \rho_{cc}(t)$; red dotted line] obtained at the tail end of the pulse ($t = t_{p0} + \tau_p$). We observe that at $I_{d0} \sim 4 \times 10^{14}$ W/m^2, the ground and excited states are exactly balanced [i.e., $\rho_{aa}(t) - \rho_{cc}(t) = 0$(t)], and $A_{\rm int}$ is halved compared to that at $I_{d0} = 10^{10}$ W/m^2. With a further increase in I_{d0} ($>4 \times 10^{14}$ W/m^2), the molecular system switches from the absorptive to transient-gain regime, and hence, $A_{\rm int}$ drops by almost two orders of magnitude and oscillates thereafter. Such behavior is due to the onset of Rabi oscillations in the molecular population, as described earlier. This transition from a slow decrease in absorption to a Rabi-oscillation regime is characteristically similar to absorption saturation in the cw regime [23]. Hence, we identify that the transition from the absorptive to gain regime causes saturation of absorption in ultrafast excitation of TLS. Note that unlike the dependence on the effective decay rate in the cw excitation regime, the saturation condition in the ultrafast regime depends only on the dipole strength of the target molecule.

Next, we numerically calculate $A_{\rm int}(t \to \infty)$ and fluorescence $F_{\rm int}(t \to \infty)$ given in Eqs. (5) and plot them in Figs. 5(a) and 5(b) as a function of the peak intensity of the drive pulse to study their saturation behavior. Note that

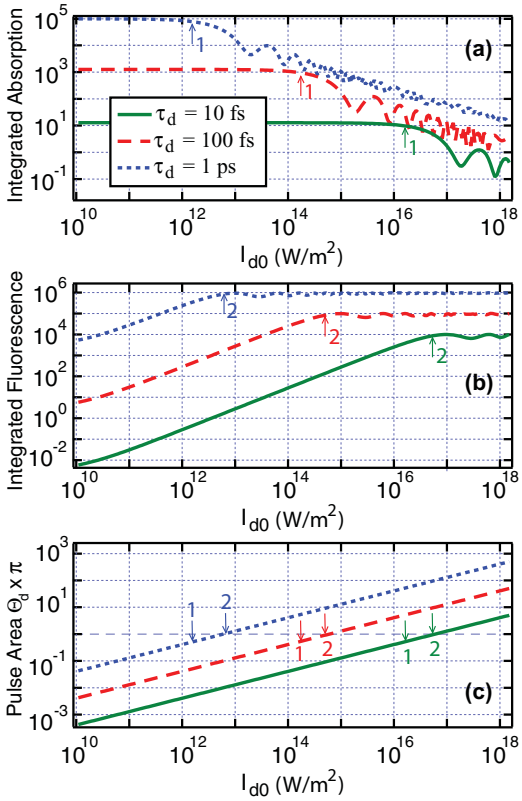

FIG. 5. (Color online) (a) Absorption saturation of a weak ultrafast probe, (b) fluorescence saturation in a TLS as a function of the peak intensity I_{d0} of drive fields of different durations, and (c) pulse area Θ_d associated with the pump pulse.

here the integration is carried out over the whole pulse, and E_w is set to zero in Fig. 5(b) to calculate the integrated fluorescence. For a range of drive intensities I_{d0}, the probe absorption remains relatively constant, and the fluorescence increases; then at high intensity both of them saturate. Longer τ_d pushes the saturation threshold toward a lower drive intensity for both absorption and fluorescence. Such pulse-duration dependence can be understood as follows: in an underdamped regime, for a given peak intensity, when the pulse duration is increased, Θ_d will increase; hence, the number of Rabi cycles will increase within the pulse duration compared to that in the shorter-pulse-duration regime. When the transient pulse area of the drive field reaches $\theta_d(t) = \pi/2$, the population inversion reaches zero ($\rho_{aa} - \rho_{cc} = 0$). Any further increase of I_{d0} can drive the population imbalance, favoring a transient gain; for example, at $\theta_d(t) \approx \pi$, we get $\rho_{aa} \to 1$, which causes a two-orders-of-magnitude reduction in the integrated absorption $A_{\rm int}(t \to \infty)$. As discussed earlier, after $\theta_d = \pi/2$ the molecular system moves from a purely absorptive to transient-gain regime. Furthermore, $A_{\rm int}(t)$ goes through cycles, with peaks when $\theta_d(t)$ is an odd integral multiple of $\pi/2$ and dips when it is an odd multiple of π. All these arguments based on θ_d can be extended to the plot of integrated absorption $A_{\rm int}$ vs the total pulse area Θ_d. Similarly, in Fig. 5(b), the integrated fluorescence $F_{\rm int}(t \to \infty)$ reaches a maximum at $\Theta_d \approx \pi$ and a minimum at $\Theta_d \approx 2\pi$; for the same reason as described earlier, the fluorescence also oscillates as

a function of I_{d0}. The integrated fluorescence is higher for the longer pulse because repumping of the excited state can occur within the pulse duration. To calculate the number of population cycles involved within the duration of the pulse for a given peak intensity of the pulse, we plot the pulse area Θ_d as a function of peak intensity for different pulse durations in Fig. 5(c). To distinguish the thresholds for absorption and fluorescence, we have added arrows marked 1 for absorption saturation and 2 for fluorescence saturation in Figs. 5(a)–5(c). Thus, for each of the pulse durations, the saturation conditions for absorption and fluorescence are given by $\Theta_d > \pi/2$ and $\Theta_d > \pi$, respectively. Also, for any given pulse duration, the threshold for absorption and fluorescence differ by a factor of 2. Note that the absorption saturation condition determined from the population inversion at a given time (in Fig. 4) differs slightly compared to the condition derived from the pulse area because the latter is integrated over the whole pulse, whereas the former relies on the population condition only at $t = t_{p0} + \tau_p$ for a given I_{d0}.

Furthermore, from Eq. (4), a condition for the absorption (fluorescence) saturation threshold can be obtained by setting $\Theta_d > \pi/2$ ($\Theta_d > \pi$). Thus, in terms of measurable parameters, the saturation threshold of the absorption and fluorescence can occur in a TLS if

$$\kappa_A\sqrt{I_{d0}}\tau_d > 1, \quad \kappa_F\sqrt{I_{d0}}\tau_d > 1, \tag{9}$$

respectively. Here, $\kappa_A = 2^{5/2}\wp_{ab}/(\hbar\sqrt{\pi c\epsilon_0})$ and $\kappa_F = \kappa_A/2$ are medium-dependent constants. The threshold intensities of the drive field that push the absorption and fluorescence to saturation are obtained as

$$\left(I_{d0}^{th}\right)_{Ab} = \frac{1}{\kappa_A^2\tau_d^2}, \quad \left(I_{d0}^{th}\right)_{Fl} = \frac{1}{\kappa_F^2\tau_d^2}. \tag{10}$$

Thus, the threshold intensity of the drive pulse for absorption or fluorescence saturation scales as the inverse of the square of the pulse duration. The shorter the pulse duration, the higher is the threshold of saturation intensity.

It may be noted that the threshold criterion for fluorescence is clearly defined by the condition where the excited population reaches the maximum value. But since the integrated probe absorption $A_{\rm int}$ monotonically decreases (at different rates) until it reaches an oscillatory regime, there is a lack of rigor in determining the *exact* threshold condition for the absorption saturation, which is also the case for absorption saturation in the cw regime [23]. Nevertheless, depending on the experiment or phenomena of interest, the above formulation can be employed to determine the threshold for ultrafast absorption saturation. For example, if a lower bound for the absorption threshold is necessary where the population inversion can only be limited to -0.9, then the new threshold can be obtained using $\Theta_d \gtrsim \pi/7$ (corresponding to $I_{d0} \sim 1.3 \times 10^{13}$ W/m^2) in Eq. (4) to obtain the new threshold conditions $(I_{d0}^{th})'_{Ab} = (2/7)^2(\kappa_A\tau_d)^{-2}$.

An important inference that can be drawn from Eq. (10) is as follows: for the discussed range of pulse durations, there exists a scaling law that can help determine the threshold intensity. To understand it better, we plot the integrated absorptions from Fig. 5(a) as a function of the pulse area of the drive pulse Θ_d in Fig. 6. For different pulse durations, even though the magnitudes of the integrated absorption are different,

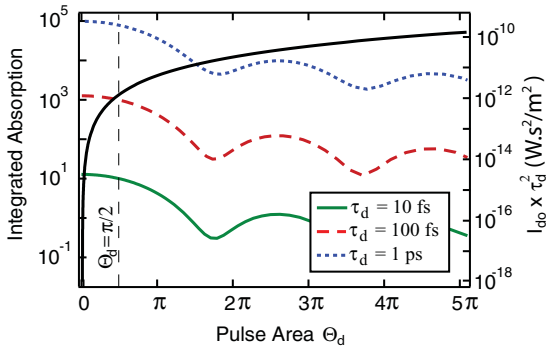

FIG. 6. (Color online) Integrated probe absorption $A_{\rm int}$ of weak probes in the TLS as a function of pulse area of the drive Θ_d plotted for three pump pulses with different durations. The scaling constant $I_{d0} \times \tau_d^2$ (solid black curve) corresponding to all three pump-pulse conditions match exactly.

there are some characteristic similarities in the plots of the integrated probe absorption. (1) The probe absorption shows sinusoidal oscillations with frequencies that are independent of the pulse durations. (2) Absorption saturation occurs at $\Theta_d \sim \pi/2$, beyond which the integrated probe absorption begins to decline rapidly and recovers near $\Theta_d \sim 2\pi$. The oscillation continues for several periods. Note that for very large pulse areas ($\Theta_d > 10\pi$), the Rabi oscillation becomes comparable to the optical frequency and vibrational period of the molecule, and hence, the RWA fails [16]. Also, according to Eq. (10), the products of the threshold peak intensity and the square of the duration of the drive pulse $[(I_{d0}^{th})_{Ab}\tau_d^2]$ should coincide, irrespective of the duration of the drive pulse. In Fig. 6, we plot this product $I_{d0}\tau_d^2$ as a function of Θ_d to show that the product converges to one line (solid black line) for all values of τ_d. The intersection point of the curve $I_{d0}\tau^2$ with $\Theta_d = \pi/2$ defines the absorption saturation threshold for TLS excited by ultrashort pulses of arbitrary duration.

This calculation can be applied to a host of resonant processes. For example, in electronic-resonant-enhanced coherent anti-Stokes Raman spectroscopy (ERE-CARS), the pump and Stokes pulses are in two-photon resonance with the molecular Raman transition, whereas they are highly detuned from the electronic transition [17], but the probe field resonantly couples the electronic transitions. The ERE-CARS technique has been extremely useful in measuring the concentration of minor species [26]. In such an experiment, while it is important to maintain the spectroscopic signature of the molecule in the generated ERE-CARS signal, saturation can alter the spectral lines [27], requiring additional correction algorithms like those employed in the saturation of fluorescence [28]. With careful detection of the ERE-CARS signal, the threshold probe intensity for saturation can be measured. The threshold probe intensity for saturation of ultrafast ERE-CARS can be calculated by treating the probe transition as a TLS and employing the above calculation to determine the threshold of fluorescence [29]. This scaling law can also be generalized to obtain saturation conditions in a variety of other resonant systems involving ultrafast laser-matter interactions, which will be published elsewhere.

IV. TWO-PHOTON PULSE AREA AND SATURATION THRESHOLD OF RAMAN COHERENCE

As an example of the generalization of the pulse-area-based threshold calculation to a two-photon-excitation system, we consider a coherent Raman transition as depicted in Fig. 2(b). When the pump E_p and Stokes E_S pulses couple to a Raman-allowed transition $v = 0 \leftrightarrow v = 1$ in the $X\,^2\Pi$ electronic manifold of NO molecules in a two-photon resonant condition, the Raman coherence ρ_{bc} is generated between the vibrational states in this model system. Saturation of Raman coherence and also the Stark shift of nanosecond-laser-excited Raman transitions have been demonstrated previously [30], where the condition for saturation is the effective two-photon Rabi frequency

$$\Omega_{2ph} = 4\frac{\Omega_p \Omega_S}{\delta} > \sqrt{\gamma\Gamma}, \tag{11}$$

where δ is the detuning of the pump and Stokes pulses from the excited electronic state. It was shown that for nanosecond excitation, a nearly saturated signal generated by beating the Raman coherence with an electronic-resonant probe facilitates quenching-independent detection of important minor gas species [31,32].

However, when the durations of the coupling laser pulses are on the order of femtoseconds, the coherence dynamics become more complex for two reasons: (1) the large bandwidth associated with femtosecond pulses can couple multiple rotational states simultaneously, and (2) the durations of the pulses are small compared to molecular decay and dephasing time scales ($\tau_i \ll \gamma^{-1}, \Gamma^{-1}$). In a previous work, we demonstrated the saturation dynamics associated with rovibrational coherent Raman processes are, in fact, dominated by saturation of pump-pulse-induced coherences between multiple purely rotational states [13]. Also, since the pulse durations are much smaller than the decays of the system, the above condition (11) of the two-photon Rabi frequency fails. However, a new criterion for saturation of the Raman process can be obtained using the pulse-area description, which is equivalent to that presented in the Sec. III. Note that for simplicity, the effect of additional rotational levels is ignored in our current three-level model.

Considering the pump and Stokes pulses to be highly detuned from the excited electronic state $|a\rangle$ (i.e., $\delta \gg \tau_p^{-1}$), the Raman process [as depicted in Fig. 2(b)] is equivalent to a two-photon absorption process between states $|b\rangle$ and $|c\rangle$. Thus, to obtain an analytical condition for the threshold of saturation of Raman coherence with ultrafast pulses, we calculate an equivalent two-photon transient pulse area associated with Ω_{2ph}, which can be defined as

$$\theta_{2ph}(t) = \frac{4}{\delta}\int_{-\infty}^{t} \Omega_p(t')\Omega_S(t')dt'. \tag{12}$$

Substituting the pump and Stokes Rabi frequencies associated with the Gaussian pulses

$$\Omega_i(t) = \Omega_{i0}(t)e^{-i(t-t_{i0})^2/\tau_i^2}(i \to p, S), \tag{13}$$

the two-photon pulse area $\Theta_{2ph} = \theta_{2ph}(t \to \infty)$ becomes

$$\Theta_{2ph} = \frac{4}{\delta}\sqrt{\frac{\pi}{\tau_p^2+\tau_S^2}}\exp\left[-\frac{(t_{p0}-t_{S0})^2}{\tau_p^2+\tau_S^2}\right]\Omega_{p0}\Omega_{S0}\tau_p\tau_S. \tag{14}$$

Clearly, the two-photon pulse area decreases exponentially as the square of the separation $|t_{p0} - t_{S0}|$ between the peaks of the pump and Stokes pulses. For $|t_{p0} - t_{S0}| \gg \tau_p^2 + \tau_S^2$, the two-photon pulse area $\Theta_{2ph} \to 0$; therefore, the saturation condition will never be reached. When the centers of the pulses overlap, the above expression reduces to

$$\Theta_{2ph} = \frac{4}{\delta}\sqrt{\frac{\pi}{\tau_p^2+\tau_S^2}}\Omega_{p0}\Omega_{S0}\tau_p\tau_S. \tag{15}$$

If one of the pulse durations is longer than the other, the above expression reduces to (assuming $\tau_p \gg \tau_S$)

$$\Theta_{2ph} = \frac{\sqrt{2\pi}}{\delta}\Omega_{p0}\Omega_{S0}\tau_S. \tag{16}$$

Thus, the shortest of the two pulses employed to excite the Raman transition will determine the saturation criterion for the Raman coherence.

Considering the durations of both pulses to be the same, i.e., $\tau_p = \tau_S = \tau$, and the pulse peaks to coincide in time, which is the usual experimental scenario in femtosecond Raman experiments, the pulse area in Eq. (14) reduces to

$$\Theta_{2ph} = \frac{\sqrt{2\pi}}{\delta}\Omega_{p0}\Omega_{S0}\tau. \tag{17}$$

Based on the criterion developed for absorption saturation in the TLS, the saturation condition for Raman coherence may be obtained as $\Theta_{2ph} > \pi/2$. Thus, under the assumptions used to derive Eq. (17), the condition for saturation of Raman coherence may be written in terms of measurable experimental parameters as

$$\kappa_{2ph}\sqrt{I_{p0}I_{S0}}\tau > 1, \tag{18}$$

where $\kappa_{2ph} = 2^{5/2}/(\pi^{1/2}\delta c\epsilon_0)$ is a medium-dependent constant. Therefore, the threshold pump-pulse intensity for Raman saturation is

$$\left(I_{p0}^{th}\right)_{\mathrm{Ram}} = \frac{1}{\kappa_{2ph}^2 I_{S0}\tau^2}. \tag{19}$$

Thus, the shorter the pulse duration, the higher is the threshold intensity for Raman saturation.

To verify this analytical form, we calculate the Raman coherence by numerically solving the coupled density-matrix equations for the three-level Raman model system. We plot the numerical values of the Raman coherence at the tail end of the pulse $|\rho_{bc}(t \gg \tau)|$ as a function of the peak intensity of the pump (maintaining the Stokes intensity at 4×10^{15} W/m^2) in Fig. 7(a) and the corresponding two-photon pulse area Θ_{2ph} in Fig. 7(b). All molecular NO parameters are the same as discussed in the previous section. We show that the Raman coherence in Fig. 7(a) saturates when the pulse area $\Theta_{2ph} \sim \pi/2$. Also, as predicted in Eq. (19), the Raman coherence saturates at higher laser intensities for shorter pulse durations. For clarity, we have added arrows marked 1 and 2 for saturation thresholds predicted numerically corresponding to $\tau_p = 1$ ps and 100 fs, respectively. Although the saturation thresholds observed in the plots are qualitatively well predicted in Eq. (18), they do not agree well quantitatively. In particular, for longer pulses, the analytical form (18) underpredicts the saturation threshold, whereas it overpredicts the threshold for

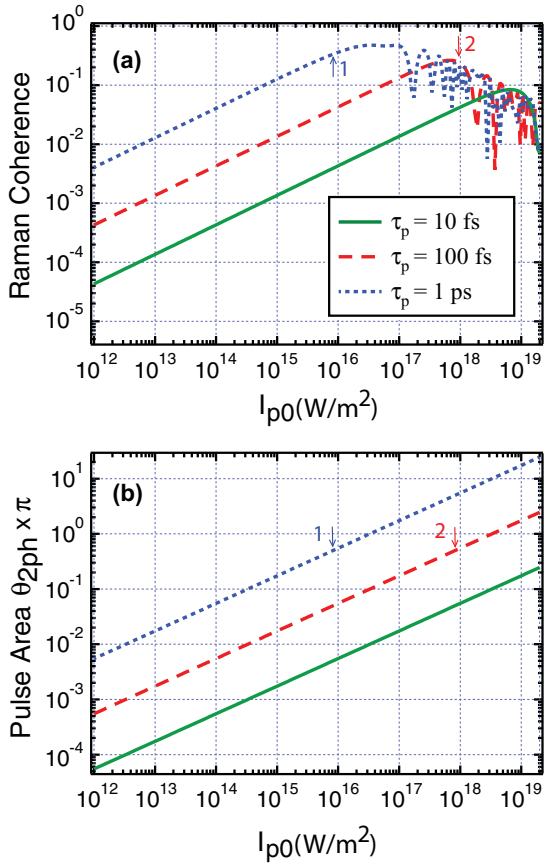

FIG. 7. (Color online) (a) Saturation of Raman coherence for different pump-pulse durations. (b) Two-photon pulse area Θ_{2ph} corresponding to different peak intensities of the pump pulse.

the shorter-duration regime. Note this description assumes a Raman process is equivalent to a TLS absorption with a two-photon Rabi frequency. A rigorous Maxwell-Bloch equation must be developed and solved analytically to obtain better quantitative agreement. It may also be observed that for a picosecond pump, the saturation value of the Raman coherence reaches the near-maximum value of 0.5, but for shorter pulses, the Raman coherence never reaches the maximum coherence value. Such a reduction in the maximum coherence value occurs because a shorter-duration pump pulse drives the system toward the highly underdamped regime where the coupling between driving pulses and the molecular state is reduced significantly. Therefore, the magnitude of the maximum achievable Raman coherence decreases.

Even though the analytical result for the Raman process predicts a saturation threshold that differs from the numerical results, the difference is within an order of magnitude. This result will therefore be extremely useful for estimating design parameters for a Raman setup to operate either in below- or above-saturation threshold limits. Again, this condition demonstrates we can generalize the pulse-area-based calculation to predetermine the threshold parameters for a wide range of pulse durations. Also, it may be used to calculate saturation in multiphoton processes, such as in two-photon fluorescence experiments to detect radicals [33] and to achieve interference-free imaging [34], for which it is vital to know the threshold for ionization. Also, such threshold calculations are important for higher-order parametric four-wave-mixing processes that are used to obtain time-resolved and collision-independent detection of minor species [35].

V. SUMMARY

In summary, we have shown that the saturation of optical processes excited by ultrafast lasers occurs in a highly underdamped regime. Using the pulse-area interpretation, we have demonstrated that the threshold for saturation follows a scaling law for a range of pulse durations. For one-photon processes, such as absorption and fluorescence, and two-photon processes, such as the coherent Raman process, the threshold drive intensity for saturation can be analytically estimated, and it is inversely proportional to the square of the pulse duration. The ultrafast saturation threshold for absorption is marked by a transition from a purely absorptive to transient-gain regime, while that for fluorescence is marked by a maximum population-inversion condition. This method can be extended to calculate other optimized pulse shapes that are promising for tailoring the saturation behavior of a system. These analytical results will be useful for estimating the design parameters of an experimental setup *a priori* for spectroscopic experiments that operate at below- or above-threshold limits of saturation.

ACKNOWLEDGMENTS

Funding for this study was provided by the U.S. Air Force Research Laboratory (Contracts No. F33615-03-D-2329 and No. FA8650-12-C-2200) and the U.S. Air Force Office of Scientific Research. This manuscript has been cleared for public release (No. 88ABW-2014-3989). The authors would like to thank Dr. H. Stauffer for his in-depth comments and stimulating discussions.

[1] M. Sargent III, Phys. Rep. **43**, 223 (1978).
[2] R. W. Boyd, *Nonlinear Optics* (Academic, San Diego, 1992).
[3] W. Demtroder, *Laser Spectroscopy*, Vol. 2, Experimental Techniques (Springer, Berlin, 2008).
[4] S. L. McCall and E. L. Hahn, Phys. Rev. Lett. **18**, 908 (1967).
[5] F. A. Hopf, G. L. Lamb, C. K. Rhodes, and M. O. Scully, Phys. Rev. A **3**, 758 (1971).
[6] M. Crisp, Phys. Rev. A **1**, 1604 (1970).
[7] J. H. Eberly, Opt. Express **2**, 173 (1998).
[8] S. Hughes, Phys. Rev. Lett. **81**, 3363 (1998).
[9] H. Kim, R. Bose, T. C. Shen, G. S. Solomon, and E. Waks, Nat. Photonics **7**, 373 (2013).
[10] R. Kienberger and F. Krausz, in *Few-Cycle Laser Pulse Generation and Its Applications*, edited by F. X. Kärtier (Springer, Berlin, 2010), p. 343.

[11] S. Roy, J. R. Gord, and A. K. Patnaik, Prog. Energy Combust. Sci. **36**, 280 (2010).
[12] G. Heck, A. Filin, D. A. Romanov, and R. J. Levis, Phys. Rev. A **87**, 023419 (2013).
[13] A. K. Patnaik, S. Roy, and J. R. Gord, Phys. Rev. A **87**, 043801 (2013).
[14] L. Yuan, G. O. Ariunbold, R. K. Murawski, D. Pestov, X. Wang, A. K. Patnaik, V. A. Sautenkov, A. V. Sokolov, Y. V. Rostovtsev, and M. O. Scully, Phys. Rev. A **81**, 053405 (2010).
[15] P. R. Berman, L. Yan, K.-H. Chiam, and R. Sung, Phys. Rev. A **57**, 79 (1998).
[16] G. M. Genkin, Phys. Rev. A **58**, 758 (1998).
[17] A. K. Patnaik, S. Roy, J. R. Gord, R. P. Lucht, and T. B. Settersten, J. Chem. Phys. **130**, 214304 (2009).
[18] F. Grossman, *Theoretical Femtosecond Physics* (Springer, Berlin, 2008), Chap. 3.
[19] A. Pusch, J. M. Hamm, and O. Hess, Phys. Rev. A **85**, 043807 (2012).
[20] T. Mishina and Y. Masumoto, Phys. Rev. Lett. **71**, 2785 (1993).
[21] D. Burnham and R. Chiao, Phys. Rev. **188**, 667 (1969).
[22] J. Lim, K. Lee, and J. Ahn, Opt. Lett. **37**, 3378 (2012).
[23] R. W. Boyd, M. G. Raymer, P. Narum, and D. J. Harter, Phys. Rev. A **24**, 411 (1981).
[24] G. S. Agarwal, *Quantum Optics* (Cambridge University Press, New York, 2013), Chap. 18.5.
[25] J. Hodgkinson and R. P. Tatam, Meas. Sci. Technol. **24**, 012004 (2013).
[26] S. Roy, W. D. Kulatilaka, S. V. Naik, N. M. Laurendeau, R. P. Lucht, and J. R. Gord, Appl. Phys. Lett. **89**, 104105 (2006).
[27] N. Chai, R. P. Lucht, W. D. Kulatilaka, S. Roy, and J. R. Gord, J. Chem. Phys. **133**, 084310 (2010).
[28] R. Altkorn and R. Zare, Annu. Rev. Phys. Chem. **35**, 265 (1984).
[29] A. K. Patnaik, J. R. Gord, and S. Roy (unpublished).
[30] L. A. Rahn, R. L. Farrow, M. L. Koszykowski, and P. L. Mattern, Phys. Rev. Lett. **45**, 620 (1980).
[31] A. K. Patnaik, S. Roy, R. P. Lucht, and J. R. Gord, J. Mod. Opt. **55**, 3263 (2008).
[32] J. P. Kuehner, S. V. Naik, W. D. Kulatilaka, N. Chai, N. M. Laurendeau, R. P. Lucht, M. O. Scully, S. Roy, A. K. Patnaik, and J. R. Gord, J. Chem. Phys. **128**, 174308 (2008).
[33] H. U. Stauffer, W. D. Kulatilaka, J. R. Gord, and S. Roy, Opt. Lett. **36**, 1776 (2011).
[34] W. D. Kulatilaka, J. R. Gord, V. R. Katta, and S. Roy, Opt. Lett. **37**, 3051 (2012).
[35] H. U. Stauffer, W. D. Kulatilaka, S. Roy, and J. R. Gord (unpublished).